CHEMISTRY
A EUROPEAN JOURNAL

DOI: 10.1002/chem.200903277

Small Noncytotoxic Carbon Nano-Onions: First Covalent Functionalization with Biomolecules

Joanna Luszczyn,[a] Marta E. Plonska-Brzezinska,*[a] Amit Palkar,[b] Alina T. Dubis,[a] Agneta Simionescu,[c] Dan T. Simionescu,*[c] Beata Kalska-Szostko,[a] Krzysztof Winkler,[a] and Luis Echegoyen*[b]

Abstract: Small carbon nano-onions (CNOs, 6–8 shells) were prepared in high yield and functionalized with carboxylic groups by chemical oxidation. After functionalization these nanostructures were soluble in aqueous solutions. 3-(4,5-dimethylthiazol-2-yl)-5-(3-carboxymethoxyphenyl)-2-(4-sulfophenyl)-2 tetrazolium (MTS) tests showed excellent cytocompatibility of all CNOs analyzed at 30 and 300 $\mu g\,mL^{-1}$, so these carbon nanostructures can be safely used for biological applications. The first covalent functionalization of oxidized CNOs (ox-CNOs) with biomolecules, by using biotin–avidin interactions is reported here. Multilayers were prepared on a gold surface by layer-by-layer assembly and the process was monitored by surface plasmon resonance (SPR) spectroscopy and atomic force microscopy (AFM). Covalent binding of molecules to the short amine-terminated organosulfur monolayers was assessed by Fourier transform infrared spectroscopy using total attenuated reflactance mode (FT-IR/HATR).

Keywords: carbon nano-onions · cytotoxicity · fullerenes · nanostructures · proteins · sensors

Introduction

Most of the structures occurring in nature arise through hierarchical ordering of atoms and molecules through self-assembly. Nature provides rich examples of elegantly organized functional nanomaterials in biological systems. We are close to understanding the driving forces, associated chemistries, and assembly strategies for the integration of artificially prepared nanoparticles into functional nanobiosystems. This knowledge has been hampered in the recent past by difficulties associated with the synthesis of materials with well-defined and reproducible physical and chemical properties.

In the last decade, significant progress in the potential applications of carbon nanostructures, especially of graphene[1] and carbon nanotubes (CNTs),[2] in biotechnology were observed.

Graphene has a two-dimensional carbon structure with very unique properties: an ambipolar electric field effect along with ballistic conduction of charge carriers,[1b] a quantum Hall effect at room temperature,[1c–e] a tunable band gap,[1f] and high elasticity.[1g] Many applications of graphene in sensors,[1h–j] transistors,[1k] and solar cells[1j] have been reported recently.

Carbon nanotubes are useful materials for a variety of biomedical applications, particularly in biosensing and optical imaging, as well as in designing novel therapeutic strategies.[2a–h] Despite the progress, there are still numerous challenges related primilary to issues of the reproducible fabrication of CNTs with well-defined structures and physicochemical properties.[2a] Some of these problematic issues include the prevention of nanotube aggregation during electrode modification, the effective separation of semi-conducting from conducting tubes, and separation of nanotubes of

[a] J. Luszczyn, Dr. M. E. Plonska-Brzezinska, Dr. A. T. Dubis, Dr. B. Kalska-Szostko, Prof. Dr. K. Winkler
Institute of Chemistry, University of Bialystok
Hurtowa 1, 15-399 Bialystok (Poland)
Fax: (+48) 85-747-0113
E-mail: mplonska@uwb.edu.pl

[b] Dr. A. Palkar, Prof. Dr. L. Echegoyen
Department of Chemistry, Clemson University
219 Hunter Laboratories, Clemson, SC 29634 (USA)
Fax: (+1) 864-656-6613
E-mail: luis@clemson.edu

[c] Dr. A. Simionescu, Dr. D. T. Simionescu
Department of Bioengineering, Clemson University
501 Rhodes Engineering Research Center
Clemson, SC 29634 (USA)
Fax: (+1) 864-656-4466
E-mail: dsimion@clemson.edu

Supporting information for this article is available on the WWW under http://dx.doi.org/10.1002/chem.200903277.

uniform lengths. These problems still demand extensive investigation of new nanomaterials.

Covalent functionalization of carbon nanostructures has been described in detail for carbon nanotubes,[2i–l] graphene,[11,m] and diamond materials.[3] It has been observed that the reactivity of fullerene-like structures decrease with increasing size of the molecule due to a decrease in the curvature.[4] While the various forms of CNTs are chemically inert, their ends and sidewalls can be functionalized by a variety of chemical groups. Small cabon nano-onions (CNOs, 6–8 shells) are potentially better systems, because they show higher reactivity and solubility in many solvents.[5] The ability to functionalize small CNOs opens up the posibilities to develop chemical sensors and biosensors. The real surface of small CNOs is also larger in comparison to the surface of other carbon nanomaterials. Therefore, better amplification of the analytical signals should be observed for CNOs, if they are used as a component of biosensors. Additionally, the diameter (5–6 nm) of CNOs enables their use for in vitro and in vivo biological studies.

The use of CNO particles for biosensors preparation requires modification of their surfaces. The CNOs were functionalized by using the method of Lieber's et al. for surface modification of single-walled nanotubes (SWNTs).[6] This derivatization method transforms the defective sites on the surface into carboxylic groups by oxidation. The oxidized CNO particles are then capable to be covalently attached to other molecules through amide-bond formation. In the past, building biosensors with immobilized oxidized nanotubes was based on the avidin–biotin interactions. This system is very well established and is characterized by very strong noncovalent interactions ($K_a = 10^{15}\,\mathrm{mol\,L^{-1}}$) between protein and ligand.[7] Avidin (MW = 67000) is a tetrameric glycoprotein that contains four specific binding sites.[8] Cooperative, multiple, noncovalent interactions are essential for realizing a strong complexation by aromatic residues, resulting in the formation of multiple hydrogen bonds, as well as van der Waals interactions.[9] Since Bayer and Wilchek[10] used biotinylated lectins and antibodies to localize receptors on erythrocyte membranes and introduced the term affinity cytochemistry, the avidin–biotin interaction method has become increasingly popular for a variety of specific applications and technologies, especially in biochemical and biomedical applications,[11,12] including analytical ones.[11c–e] Biotin (D-(+)-hexahydro-2′-oxo-2*H*-thieno[3,4-*d*]imidazole-4-pentanoic acid), which serves as coenzyme in carbon dioxide transfer, is a naturally occurring vitamin found in every living cell.[11a]

Here, for the first time, covalent functionalization of small carbon nano-onions with biomolecules by using avidin and vitamin H (biotin) interactions is reported. The potential application of nanomaterials in biosystems requires non-toxicity. In this study, we also report for the first time the cytotoxic properties of small CNOs. Chen et al.[13] investigated cytotoxicity of large CNOs on human skin fibroblasts. They reported that large CNOs can seriously impact cellular functions during maintenance, growth, and differentiation.

Our fundamental interest in the properties of CNOs modified with carboxylic groups, has been driven by their ability to interact/react with other functional compounds. As mentioned above, the oxidized CNOs can be used as a matrix for fabricating novel supramolecular architectures. We combined the use of Fourier transform infrared spectroscopy/horizontal attenuated total reflectance (FT-IR/HATR), surface plasmon resonance spectroscopy (SPR), and atomic force microscopy (AFM) to obtain complementary details of the binding events.

Results and Discussion

Biocompatibility test: Cytotoxicity of CNOs and their derivatives, oxidized CNOs (ox-CNOs), polyethylene glycol functionalized CNOs (CNOs-PEG) were exposed to fibroblasts for 4 h, which is an adequate exposure time for cytotoxicity studies.[14] For these studies we used the 3-(4,5-dimethylthiazol-2-yl)-5-(3-carboxymethoxyphenyl)-2-(4-sulfophenyl)-2 tetrazolium (MTS) test, which is a widely used colorimetric method for determining the number of viable cells in proliferation, cytotoxicity, or chemosensitivity assays. The assay employs a tetrazolium compound electron acceptor MTS and an electron coupling reagent (phenazine ethosulfate, PES), which draws electrons from the mitochondrial respiratory oxidative chain, and directly evaluats the state of mitochondrial energy production.[14] MTS diffuses rapidly through cell membranes and is reduced by NADPH/NADH, which is produced by active mitochondrial dehydrogenases.[15] The reduced MTS compound is water soluble and thus can be measured by colorimetry.[16]

Results showed excellent cytocompatibility of all CNOs tested at 30 and 300 $\mu g\,mL^{-1}$ (Figure 1). Almost 100% viability and minor reduction ($\approx$15%) in viability at 3000 $\mu g\,mL^{-1}$ was observed. Overall the results indicate that CNOs are not cytotoxic and can be safely used in biological applications.

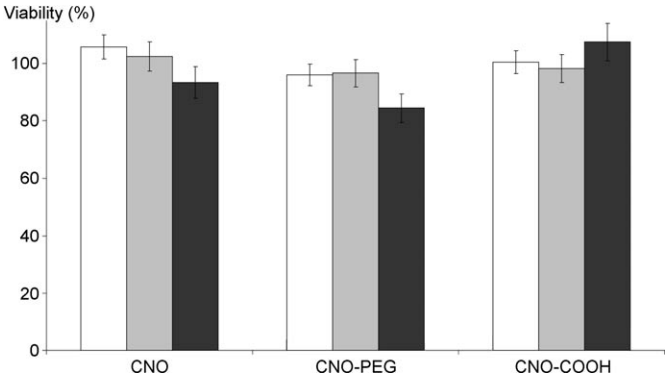

Figure 1. Viability of fibroblasts after being exposed to three concentrations (white bar: 30 $\mu g\,mL^{-1}$, gray bar: 300 $\mu g\,mL^{-1}$, black bar: 3000 $\mu g\,mL^{-1}$) of n-CNOs (where n denotes non-modified) and modified CNOs (CNO-PEG and ox-CNO). Viability was tested by using the MTS assay.

Covalent functionalization of ox-CNOs with biomolecules: Scheme 1 shows four procedures applied for the covalent functionalization of ox-CNOs incorporated into self-assembled monolayer (SAMs) with biomolecules (Scheme 1 a–c, e). In all procedures, the first preparation step was the formation of the SAMs of amine group-terminated alkanethiol on gold surfaces. To help organize the thiol layer on the gold surface, 1-octanol was added to the solution. The mixed thiol layer has denser packing than those prepared with cysteamine alone.[17] It was postulated that octanol fills the defect sites in the alkanethiolate monolayer.

In the first approach (Scheme 1 a), the oxidized carbon nano-onions were attached directly to the cysteamine layer through amide bonds. Reaction between cysteamine and ox-CNOs was promoted by water-soluble 1-(3-dimethylaminopropyl)-3-ethylcarbodiimide hydrochloride (EDC) and *N*-hydroxysuccinimide (NHS).[18] In this reaction, the carboxylic groups of the CNOs were transformed into reactive *N*-hydroxysuccinimate esters. Next, the biotin was linked through amide bonds to the ox-CNOs in the presence of EDC and NHS. The formed Au/thiol/ox-CNOs/biotin layers were tested for their biological activity. In this case, reaction with avidin was examined.

In the next procedures, depicted in Scheme 1 b and c, thiol-SAMs were initially covalently modified with biotin. CNOs with covalently attached avidin were incorporated onto the layer. This process was done in two ways. In a two-step procedure, avidin was attached to biotin and then the CNOs were incorporated onto the layer through amide-bond formation between avidin and the carboxylic groups of the ox-CNOs (Scheme 1 b). In the second case (Scheme 1 c), the CNOs were initially attached to avidin, the avidin-modified CNOs were then incorporated onto the SAMs.

The Au/thiol/biotin/avidin and Au/thiol/biotin/ox-CNO systems that were used as references, were prepared according to the procedures shown in Scheme 1 d and e, respectively.

The conditions for the modifications were the same for all procedures. It can be expected that the sequence of ox-CNOs immobilization strongly affects the structure and properties of the formed structures.

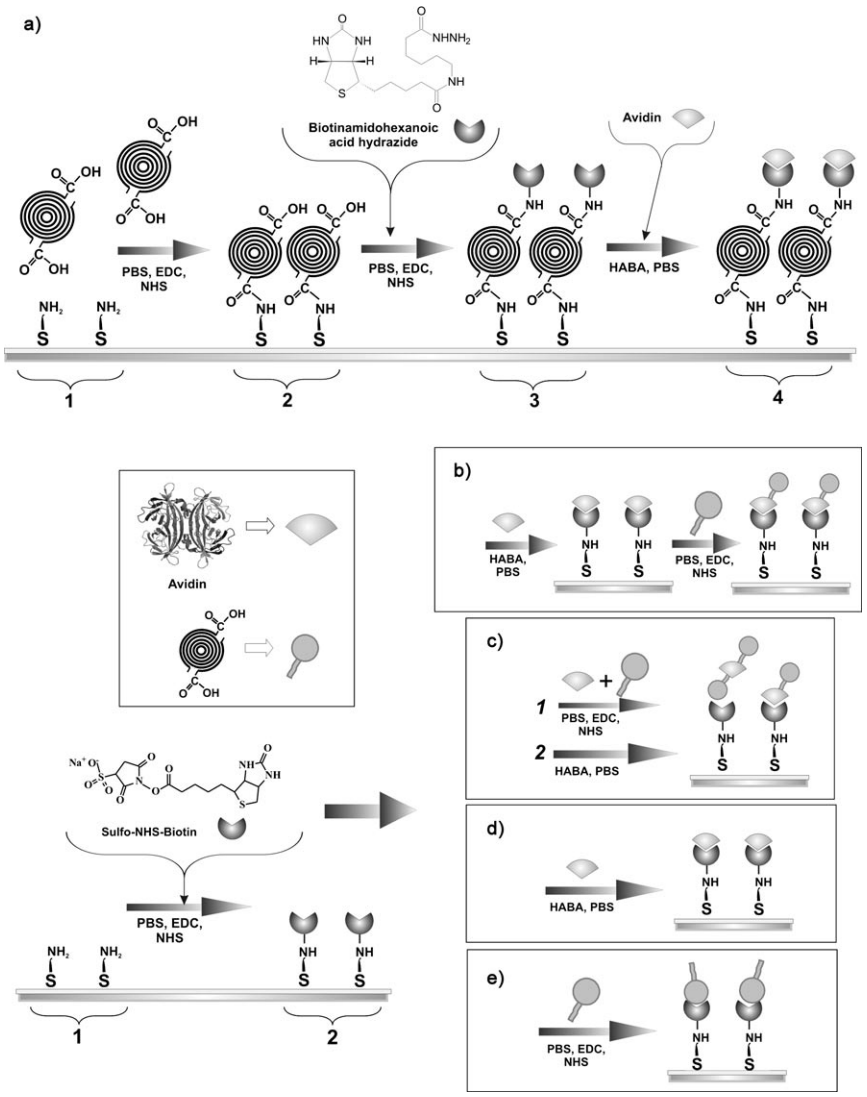

Scheme 1. Schematic illustration of the preparation of a) Au/thiol/ox-CNOs/biotin/avidin (avidin PDB ID: 2avi), b) Au/thiol/biotin/avidin/ox-CNO, c) Au/thiol/biotin/avidin + ox-CNOs, d) Au/thiol/biotin/avidin, and e) Au/thiol/biotin/ox-CNOs layers (PBS = phosphate-buffered saline, EDC = 1-(3-dimethylaminopropyl)-3-ethylcarbodiimide hydrochloride, NHS = *N*-hydroxysuccinimide, HABA = 4′-hydroxyazobenzene-2-carboxylic acid).

Fourier transform infrared spectroscopy/horizontal attenuated total reflectance (FT-IR/HATR): Fourier transform infrared spectroscopy with total attenuated reflectance mode (FT-IR/HATR) was used to monitor each step of the gold surface modification. The FT-IR/HATR spectra of functionalized ox-CNOs and CH_3COOH with biotinamidohexanoic acid hydrazide (BioAH) are shown in Figure 2 (panels I and II, respectively).

The solution-phase spectrum of ox-CNOs (Figure 2 I a) revealed a low intensity absorption band at $\tilde{\nu} = 1732\ cm^{-1}$ for the $\nu_{C=O}$ mode of the carboxylic moieties and an intense absorption at $\tilde{\nu} = 1540\ cm^{-1}$. Based on

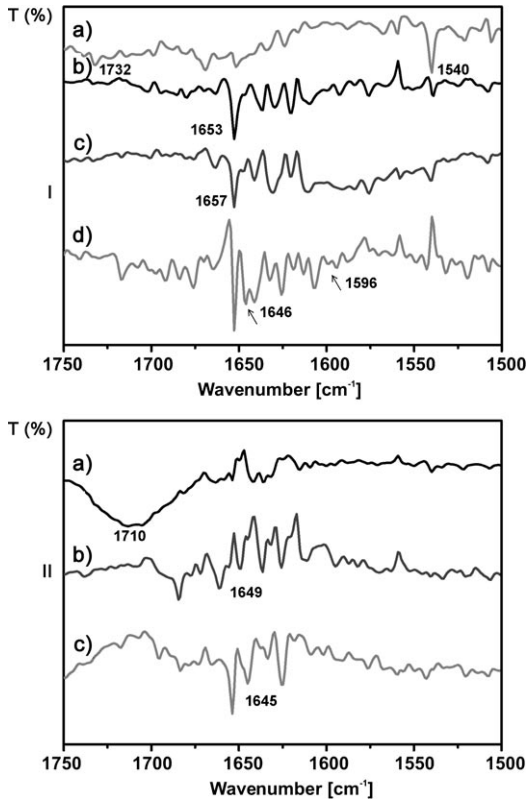

Figure 2. I) FT-IR/HATR spectra in the range of $\tilde{\nu}=1750$–$1500\ cm^{-1}$ of a) ox-CNOs in phosphate buffered saline (PBS), b) EDC/NHS in PBS solution, c) BioAH in EDC/NHS/PBS solution, and d) ox-CNOs/biotin in EDC/NHS/PBS solution. II) FT-IR/HATR spectra in the range of $\tilde{\nu}=$ 1750–1500 cm^{-1} of a) CH_3COOH in PBS, b) CH_3COOH in BioAH/PBS solution, and c) CH_3COOH/biotin in EDC/NHS/PBS solution. All spectra were corrected for the presence of the medium (PBS, EDC, and NHS).

the IR spectroscopic characterization of functionalized SWNTs,[19,20] the band detected at 1540 cm^{-1} was attributed to the C=C stretching vibration of functionalized carbons.[21–23] The spectrum of ox-CNOs treated with BioAH in the presence of EDC (Fig ure 2Id) revealed two new peaks compared to the ox-CNOs, EDC (Figure 2Ib) and BioAH/EDC (Figure 2Ic) spectra. The bands at $\tilde{\nu}=1646$ and 1596 cm^{-1} were assigned to the $\nu_{C=O}$ mode and defined as the "amide I" band and to the N–H bending vibration δ_{N-H} defined as the "amide II" band, respectively. The intensity of the N–H bending absorption is considerably weaker then the carbonyl absorption. It can be concluded that biotin is covalently linked to ox-CNOs through amide bonds.

We also analyzed the amidation reaction of CH_3COOH with BioAH as reference. Figure 2II shows the IR spectra of acetic acid (a), acetic acid in a mixture of BioAH/PBS (PBS = phosphate buffered saline) (b), and acetic acid functionalized with BioAH (c). As a result of the amidation of CH_3COOH it was found that the acidic $\nu_{C=O}$ mode was shifted from $\tilde{\nu}=1710\ cm^{-1}$ (Figure 2IIa) to $\tilde{\nu}=1645\ cm^{-1}$ (Figure 2IIc). The similarity in the position of these characteristic $\nu_{C=O}^{amide}$ absorption modes implies similar amidation reactions for both acids: ox-CNOs and CH_3COOH.

The modification of the gold surfaces was also examined by using vibrational spectroscopy. Relevant data are shown in Figure 3. Spectra of ox-CNOs and biotin-functionalized

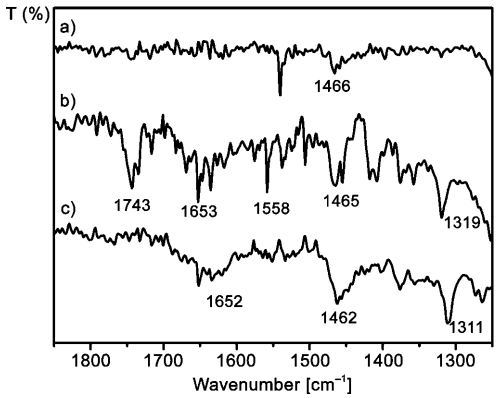

Figure 3. FT-IR/HATR spectra in the range of $\tilde{\nu}=1850$–$1250\ cm^{-1}$ of a) gold surface modified with cysteamine, b) Au/thiol/ox-CNOs, and c) Au/thiol/CNOs/BioAH.

ox-CNOs attached to the metal surface through thiolate linkage layers are presented in Figure 3b and c, respectively. The FT-IR/HATR spectrum of layers formed with cysteamine ($HS-(CH_2)_2-NH_2$) shows the characteristic bands due to deformational vibrations of NH_2 and CH_2 groups at $\tilde{\nu}=$ 1539 and 1466 cm^{-1}, respectively. After reaction with ox-CNOs the resulting spectrum revealed the characteristic D band for functionalized CNOs at $\tilde{\nu}=1319\ cm^{-1}$.[24] It was observed that the intensity of this band strongly depends on the number of hybridized carbon atoms in the nano-onions structure. The higher the number of sp^3 atoms, the larger the intensity of this absorption band. According to a recent report,[25] the appearance of a higher number of sp^3 atoms on CNOs results from the formation of defects during chemical transformation. We also observed some prominent bands for C=O stretching ($\tilde{\nu}=1743$, 1734 and 1716 cm^{-1}). These bands indicate the presence of free and hydrogen-bonded carbonyl groups. It seems likely that carboxylic groups in the outermost part of the layer may interact with each other, forming a hydrogen-bonded network.[26] The amide bands were observed at significantly lower frequencies ($\tilde{\nu}=1653$ and 1636 cm^{-1}).[27] These spectral data provide evidence for the presence of amide bonds and are consistent with the structure depicted in Scheme 1.

Next, the biotin-functionalized layers (Au/thiol/ox-CNO/biotin) were characterized. We expected that the carbonyl bands, which correspond to the carboxylic groups of the Au/thiol/ox-CNOs, would be transformed into amide carbonyls. Figure 3c shows that the resulting absorption bands are significantly broadened as a result of the growing size of the cluster.[28] The more sifnificant bands are observed at $\tilde{\nu}=$ 1652, 1462 and 1311 cm^{-1}. The appearance of the band around $\tilde{\nu}=1650\ cm^{-1}$ is typically observed for peptides and

proteins.[29] It is suggested that the band at 1652 cm^{-1} is related to the stretching vibration of the amide carbonyl group ("amide I" band). Additionally, this spectrum was compared with the spectrum of ox-CNOs treated with BioAH (Figure 2Id) and it shows that the "amide I" band is located at nearly the same frequency ($\tilde{\nu}$ = 1646 cm^{-1}). Therefore, the covalent functionalization of the carbon nano-onions with biotin can be monitored by FT-IR/HATR technique.

Atomic force microscopy (AFM): AFM is a useful tool to monitor the topography of the surface and to study interactions between the AFM tip and the sample.[30] In these experiments, we measured the topography of the SAMs by using a dynamic AFM mode (tapping mode). The AFM images of thiol-, ox-CNOs-, biotin-, and avidin-immobilized layers are shown in Figure 4 (2D) and Figure 5 (3D).

Figure 4a and Figure 5a show typical tapping mode AFM images of cysteamine layers adsorbed on a Au(111) surface. The sample was prepared as a solution in ethanol with 20 mM cysteamine. Cysteamine packs on the surface into highly ordered domains, with a typical parallel-row structure in the so-called $px\sqrt{3}$pinstripe structure[31] (Figure 5a2). Figure 4a and 5a1 show representative terrace structures with parallel edges and some zigzag shapes. Topographic cross section analysis of zigzag cysteamine layers along the AB direction are presented in Figure 4a. The distance between two neighboring zigzag structures along rows of either contrast is approximately 10 μm (distance between structures 1 and 2). The strips are composed of rows with two different contrasts in the domain (Figure 4a and 5a2). Different contrasts for the same molecules suggest that the cysteamine molecules may adsorb on the gold surface with different conformations.[30] The image root mean square (RMS) is a measure of layer roughness and a value of 7.538 nm was obtained for a 5×5 μm^2 area of cysteamine modified Au(111) surface.[32]

The cysteamine terrace structure forced the covalent attachment of ox-CNO particles to amine-terminated thiolate layers. The thiol-coated gold was exposed to a buffered solution of 100 μL ox-CNOs (5 mg mL^{-1}) for 30 min, which had been earlier activated with a mixture of EDC and NHS (0.1 M HEPES solution). The AFM images of the ox-CNOs-immobilized surfaces are shown in Figure 4b and Figure 5b. The ox-CNO particles formed pyramid-shaped domains, which resembled forest-like structures (Figure 4b, cross-section analysis along AB direction). Topographic cross-section analysis along the CD direction shows that the pyramid domains

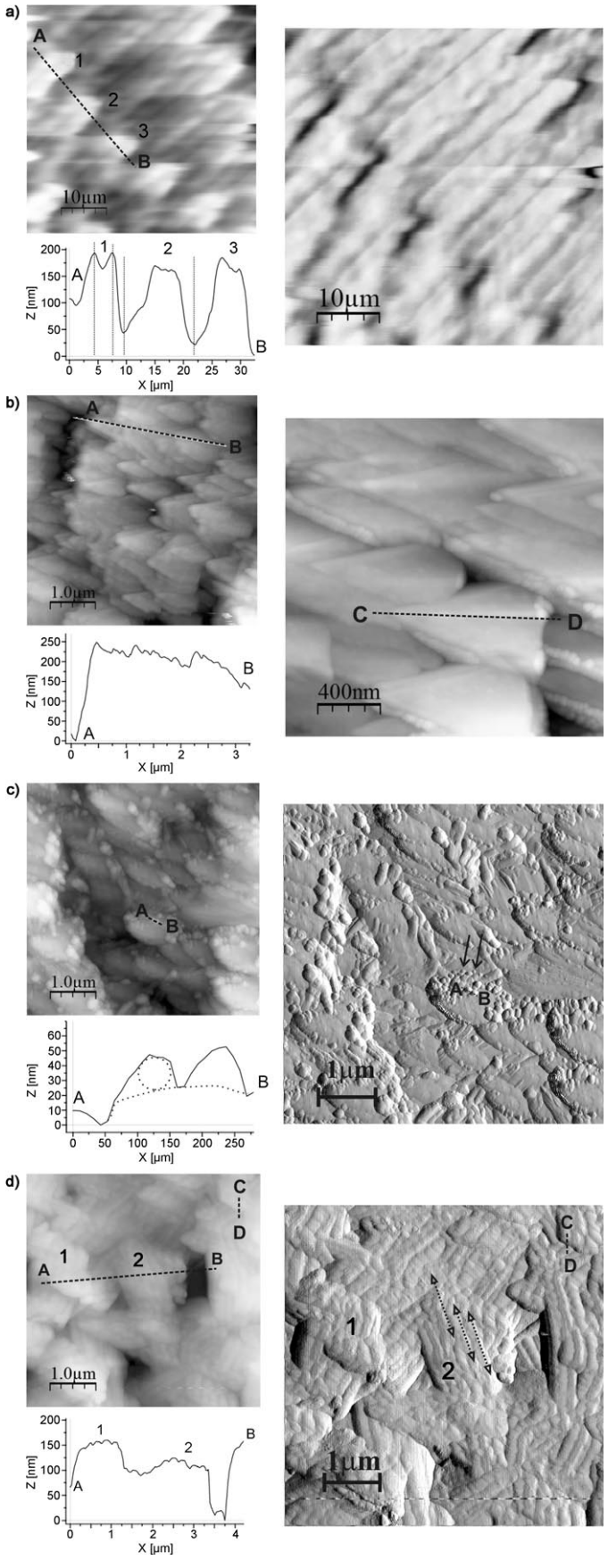

Figure 4. Tapping mode AFM images (topographic, phase, and amplitude) of a) Au(111) modified with cysteamine (Au/thiol), b) Au/thiol/ox-CNO, c) Au/thiol/ox-CNO/biotin, and d) Au/thiol/ox-CNO/biotin/avidin. Corresponding topographic cross section analyses of AFM images along the AB directions are presented in each image.

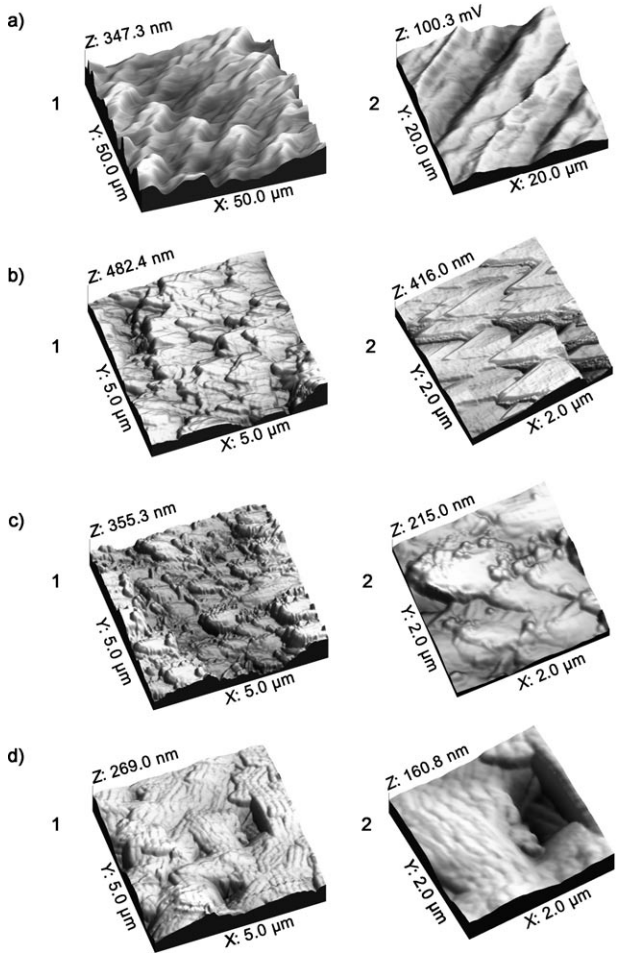

Figure 5. Tapping mode AFM images of a) Au(111) modified with cysteamine (Au/thiol), b) Au/thiol/ox-CNO, c) Au/thiol/ox-CNO/biotin, and d) Au/thiol/ox-CNO/biotin/avidin with different image size.

have a height of about 1 µm (see Figure S1 in the Supporting Information). Since the diameter of CNOs is 5–6 nm,[5a] three-dimensional pyramid structures consist of many small carbon nano-onion particles on the cysteamine layer. The strong van der Waals forces between the carbon nanoparticles lead to the self-aggregation and formation of nanoclusters on the thiol-terminated monolayers.[33] SWNTs prefer to assemble on gold surfaces as bundles of around 5–400 nm,[34] and immobilization of nanotubes is a time-dependet process.[34b] The three-dimensional pyramid structures of ox-CNOs are formed on the thiol-terminated surface with uniform arrangement and some small defects. Some of the holes visible in the CNO layers are probably forced by defects of the zigzag structures in the thiol layers. After attachment of the ox-CNOs, RMS was found to increase to 50.587 nm for a $5\times5\mu m^2$ area, indicating a rougher surface due to the presence of the CNO particles on the thiol layer.

The AFM images in Figure 4c and Figure 5c show the attachment of biotin molecules on the edges of the pyramid structures of the CNOs. Biotin molecules pack into the CNO strip domains (Figure 5c2, Figure S2 in the Supporting Information). The cross-section analysis presented in Figure 4c along the AB direction shows two neighboring biotin molecules with a diameter of around 20 nm. Biotin has a molecular size of approximately 0.5 nm.[35] The AFM image (Figure S2 in the Supporting Information) shows that biotin forms a structure consisting of domains of biotin molecules on the CNOs strips. After covalent immobilization of biotin, the roughness of the layer increases. The RMS increases from 50.587 to 56.185 nm.

The Au/thiol/ox-CNO/biotin surface was then exposed to the avidin solution ($0.45\,\mu g\,mL^{-1}$ avidin, 0.1 M HEPES buffer). In order to remove the excess of avidin, the system was washed with Tween-20 several times. Tween-20 should remove the avidin that is not specifically bound to the biotin. After washing, the surface topography was examined with AFM. Figure 4d and Figure 5d show the images after the immobilization of avidin on the biotin-modified gold surface. The morphology of the avidin surface resembles the structure of the bottom layer of biotin. Avidin is packed into ordered domains with parallel-row bundles (ca. 6 rows) with a diameter of around 1.2 µm (Figure 4d cross-section along the AB direction, bundles 1 and 2). The roughness of the surface decreased to 30.405 nm. From the topographic analysis along the CD direction the size of the monolayer of avidin was found to be about 20 nm. This value is three to four times larger than the one expected on the basis of the avidin size ($4.0\times5.5\times6.0\,nm^3$).[7] The discrepancy observed between the measured and the theoretical value is due to the AFM resolution.[36]

Surface plasmon resonance (SPR) spectroscopy: Surface plasmon resonance (SPR) spectroscopy is capable of detecting self-assembled organic monolayers and monitoring biomolecular interactions.[37,38] Materials adsorbed on surfaces change the SPR reflectivity and allows the determination of effective thicknesses of the adsorbed material.[39] SPR spectroscopy was used to sequentially monitor the assembly steps, starting with the formation of the thiol layer, the immobilization of the ox-CNO particles, biotin incorporation through amide bonds, and avidin incorporation. The quantitation is based on the variation of the SPR parameters, such as shifts of the resonance angles at the reflectance minimum (surface plasmon angle, θ_{SPR}).[39]

Films with incorporated nano-objects such as clay and supramolecular complexes,[40] metallic,[41] semiconducting,[42] or insulating nanoparticles[43] have been extensively studied by using SPR methods. Only a few articles dealing with fullerenes[44] or carbon nanotubes investigated by using SPR measurements[42] have been reported.

The mechanism of the observed amplified SPR signal is governed by various interactions among and within the organic, protein, and nanoparticle layers or changes of the structural and optical properties of such devices. SPR signals depend on the electron density, effective mass, particle shape, size, dielectric properties, and the environment.[41d]

The modifications of SPR disks were done as described in Scheme 1. After each step the SPR angular reflectance

curve (R vs. θ_{SPR} with R = reflexitivity) was collected (see Figure 6. All spectra were recorded in 0.1 M PBS buffer solution, after thoroughly rinsing the samples to remove the nonspecifically bonded biomolecules (rinsing solution: 0.1 M PBS/Tween-20). Figure 6 shows the shifts of the SPR angles measured on gold disks modified as described above. The experimentally measured shifts of the SPR angles are listed in Table 1, entries a–e. $\Delta\theta_{SPR}$ and $\delta\theta$ refer to the resonance angle between two neighboring monolayers and the difference of the resonance angles compared to a bare gold SPR, respectively.

Table 1. SPR angle shifts.

Entry	Layer	$\delta\theta_{SPR}$[a] [°]	$\triangle\theta_{SPR}$[b] [°]
	Au	0	0
	cysteamine	0.153	0.153
	ox-CNOs	1.061	0.908
a	biotin (BioAH)	1.454	0.546
	avidin	2.082	0.628
	biotin (BioNHS)	0.398	0.245
b	avidin	0.963	0.565
	ox-CNOs	1.643	0.680
c	biotin (BioNHS)	0.398	0.245
	ox-CNOs + avidin	0.516	0.118
d	biotin (BioNHS[c])	0.398	0.245
	avidin	0.963	0.565
e	biotin (BioNHS)	0.398	0.245
	ox-CNOs	1.753	1.355

[a] $\delta\theta$ refers to the difference of the resonance angles from a bare gold SPR. [b] $\triangle\theta$ refers to the difference of the resonance angles between the top layer and the neighboring layer. [c] BioNHS = biotin 3-sulfo-*N*-hydroxy-succinimide ester sodium salt.

The Au/thiol/biotin/avidin film on the SPR disk was formed according to the procedure described in Scheme 1 d. Upon formation of the mixed cysteamine/1-octanol layer, the SPR angle shifted positively around 0.153° ($\Delta\theta_{SPR}$) in comparison to the bare gold surface. After the injection of 25 μL of biotin 3-sulfo-*N*-hydroxy-succinimide ester sodium salt (BioNHS; 55 $\mu g\,mL^{-1}$ in 0.1 M HEPES buffer solution) and thoroughly rinsing with 0.1 M PBS/Tween-20, the SPR angle shifted positively by $\Delta\theta_{SPR} = 0.245°$. After formation of the biotin layer, we checked the bioactivity of the SAMs with avidin in the PBS buffer solution. The results obtained for a concentration of 0.45 $\mu g\,mL^{-1}$ of avidin are presented in Table 1 and Figure 6. The adsorption of avidin resulted in an SPR angle shift of 0.565° compared to the Au/thiol/biotin surface (Figure 7). Figure 7 b shows a real-time sensorgram of consecutive binding of avidin (gradual addition of 20 μL of a solution of 0.45 $\mu g\,mL^{-1}$ avidin in 0.1 M PBS) to a Au/thiol/biotin surface. The positive shift of the SPR angle is observed after each exposure of the Au/thiol/biotin layer to avidin. The shift of $\Delta\theta_{SPR}$ becomes smaller with the number of injections. After seven injections a saturation of the surface with avidin is observed.

The SPR method detects changes of the refractive index of thin films assembled on a gold surface and can give quantitative information of the adsorbed material.[39] Within a family of compounds (e.g., proteins), changes of θ_{SPR} correlate linearly with the mass of the adsorbed material per unit area in a similar way.[45,46] The instrument used in this study reports changes in θ_{SPR} in resonance units (RU, 1000 RU = 0.1°). The changes of the SPR response (ΔRU) associated with the adsorbed thiol, BioNHS, avidin layers are: 1530 RU, 2450 RU, and 5650 RU, respectively. According to the correlation of the SPR response with the surface protein concentration by Stenberg (1 kRU = 1 $ng\,mm^{-2}$),[47] we calculated the thickness of consecutive layers of the SAMs. The thicknesses of additional layers are: 1.04 nm (thiol), 2.33 nm (biotin), and 6.65 nm (avidin). The thickness of the protein layers can also be calculated theoretically by using the SPR angle shift and the refractive index $n_{thin\,film} = 1.5$.[39] The values of the layer thicknesses obtained in this way were: 1.5 nm (thiol), 2.5 nm (biotin), and 5 nm (avidin). Thus, there is good agreement between the thicknesses obtained by these two methods. The values for the thicknesses of the layers presented in this paper are also in agreement with values already published in the literature.[29,48,49]

The structures containing CNOs were also examined by the SPR method. The different procedures of ox-CNO incorporation into SAMs are described in Scheme 1. In every case, a positive shift of the SPR angle was observed, thus indicating that ox-CNOs are immobilized on the modified gold surface. However, the magnitude of $\Delta\theta_{SPR}$ depends on the sequence of layer-by-layer deposition. This indicates differences in the morphology and thickness of the obtained structures.

Following procedure c (Scheme 1, Table 1, entry c), the ox-CNO–avidin hybrids were immobilized on the gold surface modified with biotin. In this case, the SPR angle shift is relatively low and equal to 0.118° (Figure 6 b). By using the electrical field enhancement model, the thickness of the ox-CNOs layer was calculated to be about 1 nm. This value is much lower when compared to the size of carbon nano-onions. It is evident that Au/tiol/biotin is only partially covered by the ox-CNO–avidin hybrids. Probably, the avidin binding sites are blocked by carbon nano-onions and a non-densely packed structure is formed.

Much higher changes of $\Delta\theta_{SPR}$ were observed for the structures formed during separate deposition of avidin and ox-CNOs (procedure b, Scheme 1 and Figure 6 c). In this case, the total $\Delta\theta_{SPR}$ is equal to 1.245°. This value corresponds to the avidin/ox-CNO layer thickness of 14.75 nm. A good agreement between theoretical and experimental values indicates that avidin/ox-CNOs form a densely packed layer on the biotin surface.

The biggest shift of the SPR angle ($\Delta\theta_{SPR} = 1.355°$) was observed for ox-CNOs attached to the Au/thiol/biotin surface (Scheme 1 e, Table 1, entry e and Figure 6 d). The thickness of the layer corresponding to this $\Delta\theta_{SPR}$ value (16.12 nm) is higher than the expected thickness of a monolayer. It suggests that the surface is modified with a multilayer of ox-CNOs.

Direct deposition of ox-CNOs on the gold surface modified with cysteamine results in a positive shift of θ_{SPR} by 0.908 (Table 1, entry a and Figure 6 e), which corresponds to

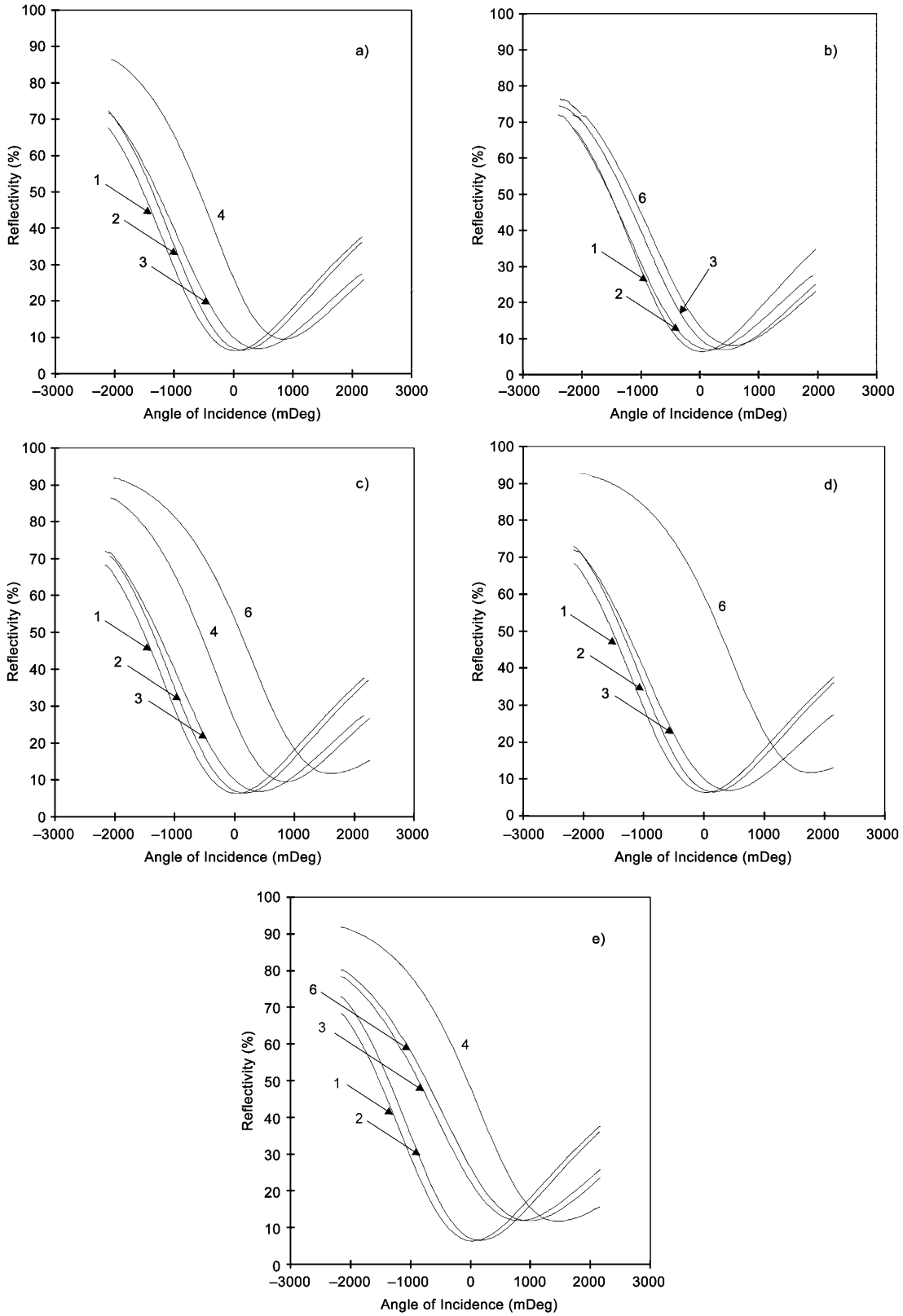

Figure 6. SPR reflectivity curves of each step of Au (1) layer modification by using cysteamine (2), biotin (3), avidin (4), ox-CNOs + avidin (5), ox-CNOs (6) in different sequences (see Scheme 1 a–e).

a thickness of 10.8 nm of the ox-CNO layers. Taking into account the average diameter of CNOs (5–6 nm) we can assume that more than a monolayer is deposited at the modified gold surface.

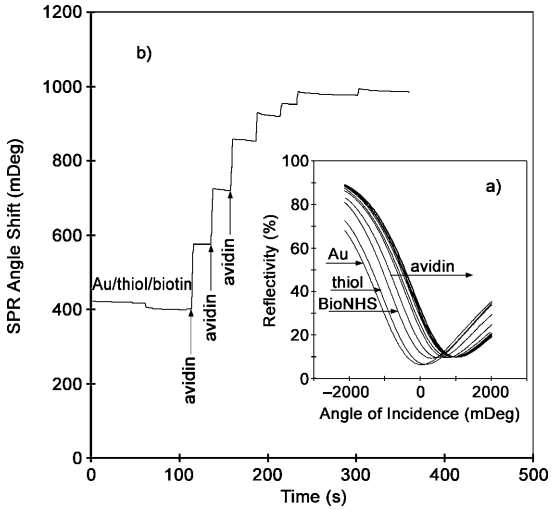

Figure 7. a) SPR experimental reflectivity curves. b) Sensorgram of layer-by-layer assembly of avidin onto an Au/thiol/biotin surface. In each step, 20 μL avidin solution (0.45 μg mL^{-1}, 0.1 M PBS) were injected to the 0.1 M PBS/Tween-20 solution. Flow rate 5 μL min^{-1}.

The sequence of ox-CNOs immobilization strongly affected the structure and properties of the resulting surfaces. Results showed that ox-CNOs can be successfully used as linking layers to amplify the analytical signal of the biosensor.

Conclusion

For the first time formation of systems containing small carbon nano-onions (CNOs) functionalized with biomolecules was demonstrated. These systems were formed by using layer-by-layer deposition methods. Gold electrodes modified with self-assembled monolayers (SAMs) of cysteamine were used as the base for immobilization of functionalized CNOs. The structure of the formed films was investigated by Fourier transform infrared spectroscop/horizontal attenuated total reflectance (FTIR/HATR), surface plasmon resonance (SPR) spectroscopy, and atomic force microscopy (AFM). All of these methods confirmed the formation of the SAMs on the gold surface. The film structure depends on the sequence of film component deposition. Protein-like molecules attached to the CNOs retain their biological activity. Additionally, biocompability tests showed that the ox-CNOs are not cytotoxic. These systems can be used for biosensor construction and for other biological applications.

Experimental Section

General: The following chemicals were used as received: polyethylene glycol (PEG 1500, Sciencelab), phosphate buffered saline (PBS, in 1 L deionized water: 0.01 M phosphate buffered saline, 0.138 M NaCl, 0.0027 M KCl, pH 7.4, Sigma–Aldrich), *N*-(2-hydroxyethyl)piperazine-*N*′-(2-ethanesulfonic acid) (HEPES, sodium salt > 99%, Fluka), 2-mercaptoethylamine hydrochloride (+98%, Alfa Aesar), 1-octanol (≥ 99.5%, Fluka), biotinamidohexanoic acid hydrazide (BioAH, min. 95% TLC, Sigma–Aldrich), biotin 3-sulfo-*N*-hydroxy-succinimide ester sodium salt (BioNHS, 90% TLC, Sigma–Aldrich), avidin from hen egg white (78%, ≈12 units mg^{-1}, Biochemika), 1-(3-dimethylaminopropyl)-3-ethylcarbodiimide hydrochloride (EDC, +98%, Alfa Aesar), *N*-hydroxysuccinimide (NHS, ≥ 97%, Fluka), isopropanol (+99%, Alfa Aesar), anhydrous ethanol (99.8%, Poch Gliwice), acetic acid (≥ 99%, Sigma–Aldrich), sulfuric acid (min. 95%, Poch Gliwice), nitric acid (65%, Poch Gliwce), dimethylformamide (99.9+%, Sigma–Aldrich), dimethyl sulphoxide (DMSO), sodium hydrogen carbonate. All aqueous solutions were prepared by using deionized water, which was further purified with a Milli-Q system (Millipore). For cytotoxicity studies, 3-(4,5-dimethylthiazol-2-yl)-5-(3-carboxymethoxyphenyl)-2-(4-sulfophenyl)-2 tetrazolium (MTS), phenazine ethosulfate (PES), and phenazine methosulfate (PMS) components of the CellTiter96 AQueous One Solution Cell Proliferation Assay Kit (Promega, Madison WI) were used. Rat dermal fibroblasts were obtained by explant technique from adult skin samples and cell culture media of phosphate buffered saline (PBS) and cell culture additives (Sigma–Aldrich).

CNOs, ox-CNOs, and CNOs-PEG: The synthesis of small CNOs (6–8 shells) was performed by annealing nanodiamonds of 5 nm average particle size under a positive pressure of helium at 1650 °C.[50] Through treatment of these carbon species with a sulfuric acid/nitric acid solvent mixture (3:1, v/v) for 10 min defective sites on the surface were transformed into carboxylic acids by oxidation. These carboxylic groups were amidated with polyethylene glycol (PEG) in the solid-state reaction applying 170 °C for 2 h.

Cytotoxicity testing of CNOs: Rat dermal fibroblasts were grown in culture medium (Dulbecco′s modified eagle medium (DMEM)), 10% fetal bovine serum, 1% antibiotics) in a cell culture incubator (95% humidity and 5% CO_2 in air) and used at passage CNOs (n-CNOs, ox-CNOs, CNOs-PEG). CNOs were first suspended into culture medium (3000 μg mL^{-1}) and then further diluted with culture medium to 300 μg mL^{-1} and 30 μg mL^{-1}. Negative control cells were exposed to culture medium alone and positive controls were treated with 70% ethanol for 30 min, which kills most cells. For testing, cells were plated in 12-well culture plates at 1×10^5 cells per well and cultured for two days in the same culture medium. On the day of testing, the medium was removed and CNOs suspended in culture medium (30, 300, and 3000 μg mL^{-1}) were added to each well. The exposure to CNOs was done for 4 h at 37 °C in the cell culture incubator. After incubation, CNOs in medium were aspirated from wells, the wells washed with PBS, and next MTS solution (from the Promega kit) was added. After 1 h at 37 °C, the media from each well were collected, diluted 15-fold and the absorbance at 490 nm was measured with a 96-well plate reader. Absorbance at 490 nm is directly proportional to the number of living cells in culture. To calculate the viability of CNO-treated cells, the absorbance of the negative control cells was used as 100% cell viability and the absorbance of the ethanol-killed cells as 0% viability. Absorbance readings at 490 nm were performed on a BioTek MicroQuant microplate reader connected to a PC and analyzed by KCJunior software. An aliquot (250 μL) from each sample were pipetted in each well of a 96-well plate and the absorbance was measured.

Biotinylation of ox-CNOs layer and interaction with avidin: All types of created biosensors by using carbon nano-onions were based on thiol-modified gold. Gold foil (Au 3N, 0.05 mm thickness), gold single crystal (Au(111), 10 mm diameter, 1–2 mm thickness), and SPR disks with thin gold layers (gold-coated glass slides, 25 mm diameter) were rinsed with anhydrous ethyl alcohol and dried (except slides for SPR measurements) under a stream of argon. Next, they were immersed into a solution of cysteamine in ethanol (20 mM for SPR and AFM measurements, 300 mM for IR measurements) with addition of 1-octanol for 2 h. A cysteamine/octanol mixture was prepared by adding octanol in a dropwise manner to a measured volume of a solution of cysteamine until no more would dissolve. This procedure usually required only a few drops of solution aliquot, about 0.50 mg mL^{-1} at 25 °C. Then modified foil and crystals were taken out of the solution, rinsed with anhydrous ethyl alcohol and distilled water and dried under argon stream. SPR disks were only rinsed with ethyl alcohol. The ox-CNOs were binded to the thiol-modified gold

surface in the following manner. A solution of ox-CNOs in ethanol (100 μL, 5 mg mL^{-1}), activated by EDC (50 μL, 100 mg mL^{-1}) and NHS (50 μL, 50 mg mL^{-1}), was added to a HEPES buffer solution (10 mL, pH 7.2). Next, cysteamine-modified foil, crystal and slides surfaces were exposed to the solution for 1 h. Then they were rinsed with HEPES buffer, dried (except the SPR disks) under a stream of argon and immersed for 1 h into HEPES buffer solution (10 mL) containing BioAH (25 μL, 50 mM in DMSO) activated by EDC and NHS (in the same volume and concentration as for ox-CNOs). Modified foils and crystals were rinsed again with HEPES buffer and dried under argon stream. SPR disks were only rinsed with HEPES buffer without drying. Finally, Au/thiol/ox-CNOs/BioAH was tried as avidin biosensor by using a reagent concentration of 0.45 μg mL^{-1}. In other biosensor structures biotin-coupled amine groups were used as molecule binding site to the thio-modified gold surface. BioNHS (50 μL, 25 mM in water), which had been activated by EDC/NHS reagents in the same way as BioAH, was added to a HEPES buffer solution (10 mL), and thiol-modified foil, crystal, and disk surfaces were exposed to the solution for 1 h. Other layers were prepared by using the procedure and concentration of chemicals as described above, but in different sequence. The next options for using ox-CNOs in biosensor construction were binding carbon nano-onions or ox-CNOs mixed with avidin directly to the BioNHS layer. The film was formed by first catching avidin with the BioNHS layer, and next binding of ox-CNOs to the Au/thiol/BioNHS/avidin layers. As a reference, a biosensor based on Au/thiol/BioNHS/avidin layers was prepared.

CH_3CONH-biotin for FT-IR/HATR measurements: BioAH (25 μL, 18.6 mg mL^{-1} in DMSO) previously activated with EDC (50 μL, 100 mg mL^{-1}) and NHS (50 μL, 100 mg mL^{-1}) and incubated overnight at room temperature, was added to a solution of 5% acetic acid (5 mL). Next, avidin (25 μL, 0.45 μg mL^{-1}) was added to the solution.

FT-IR/HATR measurements: The FT-IR spectra were recorded in the range of $\tilde{\nu}$ = 550–4000 cm^{-1} with a Nicolet Magna IR 550 Series II spectrometer at room temperature. The spectra were collected at a resolution of 4 cm^{-1}, apodized with triangular function, and zero-filling factor of 1 was applied. All the spectra were corrected with conventional software in order to cancel the variation of the analyzed thickness with the wavelength. KBr pellets containing n-CNOs or ox-CNOs were dried at 80 °C for 3 h. For the FT-IR/HATR (Fourier transform infrared spectroscopy/horizontal attenuated total reflectance) technique, a zinc selenide (ZnSe) crystal (θ = 45°, n_p = 2.4) was used. The solution of the analyzed samples was placed in HATR cells and a beam of infrared radiation entering a crystal underwent multiple internal reflections. The resultant radiation was measured and plotted as a function of the wavelength.

Surface plasmon resonance (SPR) spectroscopy: Surface plasmon resonance spectroscopy measurements were performed with an AutoLab SPRINGLE SPR system with hardware and software of Eco Chemie B.V. The SPR experiments described herein utilize the Kretschmann configuration. The glass surface of the cleaned sensor disks was pressed onto the base of a hal-cylindrical lens (ZK_7, n = 1.61) by an index matching oil (n = 1.61). The SPR spectrometer was equipped with a GaAs laser diode, λ = 670 nm. The measured $\Delta\theta$ values correspond to the amount of adsorbed material with a mass sensitivity factor of 120 mdeg per 100 ng cm^{-2}. The measurements were conducted at room temperature.

Atomic force microscopy (AFM): The atomic force microscopy was performed with a Veeco Caliber Microscope. The AFM imaging was obtained in tapping mode at 173.85 kHz. Root mean square (RMS) roughness was performed by using Nanotec Electronica WS×M 5.0 Develop 1.0 program.

Acknowledgements

We gratefully acknowledge the financial support of the State Committee for Scientific Research, Poland, projects: N N204 111535 to M.E.P.-B., N N204 246435 to B.K.-S., and N N204 374733 to K.W., the National Science Foundation, USA, Grant: DMR-0809129 to L.E. The presented material is based on work that is supported by the National Science Foundation while L.E. was working at the foundation. All opinions, findings, conclusions, or recommendations expressed herein are those of the authors and do not necessarily reflect the views of the National Science Foundation.

[1] a) C. N. R. Rao, A. K. Sood, K. S. Subrahmanyam, A. Govindaraj, *Angew. Chem.* **2009**, *121*, 7890–7916; *Angew. Chem. Int. Ed.* **2009**, *48*, 7752–7777; b) K. S. Novoselov, A. K. Geim, S. V. Morozov, D. Jiang, Y. Zhang, S. V. Dubonos, I. V. Grigorieva, A. A. Firsov, *Science* **2004**, *306*, 666–669; c) K. S. Novoselov, A. K. Geim, S. V. Morozov, D. Jiang, M. I. Katsnelson, I. V. Grigorieva, S. V. Dubonos, A. A. Firsov, *Nature* **2005**, *438*, 197–200; d) Y. Zhang, J. W. Tan, H. L. Stormer, P. Kim, *Nature* **2005**, *438*, 201–204; e) K. S. Novoselov, Z. Jiang, Y. Zhang, S. V. Morozov, H. L. Stormer, U. Zeitler, J. C. Maan, G. S. Boebinger, P. Kim, A. K. Geim, *Science* **2007**, *315*, 1379; f) M. Y. Han, B. Oezyilmaz, Y. Zhang, P. Kim, *Phys. Rev. Lett.* **2007**, *98*, 206805; g) C. Lee, X. Wei, J. W. Kysar, J. Hone, *Science* **2008**, *321*, 385–388; h) O. Leenaerts, B. Partoens, F. M. Peeters, *Phys. Rev. B* **2008**, *77*, 125416; i) N. L. Rangel, J. M. Seminario, *J. Phys. Chem. A* **2008**, *112*, 13699–13705; j) N. Varghese, U. Mogera, A. Govindaraj, A. Das, P. K. Maiti, A. K. Sood, C. N. R. Rao, *ChemPhysChem* **2009**, *10*, 206–210; k) V. C. Tung, M. J. Allen, Y. Yang, R. B. Kaner, *Nat. Nanotechnol.* **2009**, *4*, 25–32; l) Z. Liu, Q. Liu, Y. Huang, Y. Ma, S. Yin, X. Zhang, W. Sun, Y. Chen, *Adv. Mater.* **2008**, *20*, 3924–3930; m) E. Bekyarova, M. E. Itkis, P. Ramesh, C. Berger, M. Sprinkle, W. A. de Heer, R. C. Haddon, *J. Am. Chem. Soc.* **2009**, *131*, 1336–1337; n) K. S. Subrahmanyam, A. Ghosh, A. Gomathi, A. Govindaraj, C. N. R. Rao, *Nanosci. Nanotechnol. Lett.* **2009**, *1*, 28–31.

[2] a) C. N. Ram Rao, A. Govindaraj, *Nanotubes and Nanowires* (Eds.: P. O'Brien, H. Kroto, H. Craighead), RSC, Oxford, **2005**; b) Y. Xiao, F. Patolsky, E. Katz, J. F. Heinfled, I. Willner, *Science* **2003**, *299*, 1877–1881; c) R. D. Averitt, D. Sarkar, D. Halas, *J. Phys. Rev. Lett.* **1997**, *78*, 4217–4220; d) H. Gao, Y. Kong, D. Cui, C. S. Ozkam, *Nano Lett.* **2003**, *3*, 471–473; e) C. Dwyer, M. Guthold, M. Falvo, S. Washburn, R. Superfine, D. Erie, *Nanotechnology* **2002**, *13*, 601–604; f) J. Kong, H. Dai, *J. Phys. Chem. A* **2001**, *105*, 2890–2893; g) J. L. Anderson, D. W. Armstrong, G. Wei, *Anal. Chem.* **2006**, *78*, 2892–2902; h) J. S. Wilkes, *Green Chem.* **2002**, *4*, 73–80; i) Y.-Y. Ou, M. Huang, *J. Phys. Chem. B* **2006**, *110(5)*, 2031–2036; j) S. E. Baker, W. Cai, T. L. Lasseter, K. P. Weidkamp, R. J. Hamess, *Nano Lett.* **2002**, *2*, 1413–1417; k) R. Blake, Y. K. Guriko, J. Coleman, M. Cadek, A. Fonseca, J. B. Nagy, W. J. Blau, *J. Am. Chem. Soc.* **2004**, *126*, 10226–10227; l) G. N. Ostojic, J. R. Ireland, M. C. Hersam, *Langmuir* **2008**, *24*, 9784–9789.

[3] a) A. Krueger, J. Stegk, Y. Liang, L. Lu, G. Jarre, *Langmuir* **2008**, *24*, 4200–4204; b) H. Wang, J.-P. Griffiths, R. G. Edgell, M. G. Moloney, J. S. Foord, *Langmuir* **2008**, *24*, 862–868; c) J. Zhao, H. Park, J. Han, J. P. Lu, *J. Phys. Chem. B* **2004**, *108*, 4227–4230.

[4] A. Hirsch, *Top. Curr. Chem.* **1999**, *199*, 93–134.

[5] a) A. Palkar, F. Melin, C. M. Cardona, B. Elliott, A. K. Naskar, D. D. Edie, A. Kumbhar, L. Echegoyen, *Chem. Asian J.* **2007**, *2*, 625–633; b) C. T. Cioffi, A. Palkar, F. Melin, A. Kumbhar, L. Echegoyen, M. Melle-Franco, F. Zerbetto, G. M. Aminur Rahman, Ch. Ehli, V. Sgobba, D. M. Guldi, M. Prato, *Chem. Eur. J.* **2009**, *15*, 4419–4427; c) L. Zhou, C. Gao, D. Zhu, W. Xu, F. F. Chen, A. Palkar, L. Echegoyen, E. S.-W. Kong, *Chem. Eur. J.* **2009**, *15*, 1389–1396.

[6] S. Wong, A. Woolley, E. Joselevich, C. Cheung, C. Lieber, *J. Am. Chem. Soc.* **1998**, *120*, 8557–8558.

[7] a) N. M. Green, *Biochem. J.* **1963**, *89*, 585–591; b) L. Pugliese, A. Coda, M. Malcovati, M. Bolognesi, *J. Mol. Biol.* **1993**, *231*, 698–710.

[8] N. M. Green in *Advances in Protein Chemistry* (Eds.: C. B. Anfinsen, J. T. Edsall, F. M. Richards), Academic Press, New York, **1975**.

[9] M. V. Rekharsky, T. Mori, Ch. Yang, Y. H. Ko, N. Selvapalam, H. Kim, D. Sobransingh, A. E. Kaifer, S. Liu, L. Isaacs, W. Chen, S. Moghaddam, M. K. Gilson, K. Kim, Y. Inoue, *Proc. Natl Acad Sci.* **2007**, *104(52)*, 20737–20742.

[10] a) E. A. Bayer, M. Wilchek, E. Skutelsky, *FEBS Lett.* **1976**, *68(2)*, 240–244; b) Y. Hiller, J. M. Gershoni, E. A. Bayer, M. Wilchek, *Biochem. J.* **1987**, *248*, 167–171.
[11] a) M. F. Utter, D. B. Keech, *J. Biol. Chem.* **1960**, *235*, PC17–PC18; b) V. P. Torchilin, *Bioconjugate Chem.* **1999**, *10*, 146–149; c) M. Wilchek, E. A. Bayer, *Anal. Biochem.* **1988**, *171*, 1–32; d) D. C. Schriemer, T. Yalcin, L. Li, *Anal. Chem.* **1998**, *70*, 1569–1575; e) J.-S. Choi, Y.-W. Jun, S.-I. Yeon, H. Ch. Kim, J.-S. Shin, J. Cheon, *J. Am. Chem. Soc.* **2006**, *128*, 15982–15983; f) G. R. Szilvay, A. Paananen, K. Laurakainen, E. Vuorimaa, H. Lemmetyinen, J. Peltonen, M. B. Linder, *Biochemistry* **2007**, *46*, 2345–2354.
[12] a) J. A. Ascencio, A. C. Rincon, G. Canizel, *J. Phys. Chem. B* **2005**, *109*, 8806–8812; b) R. D. Carpenter, M. Andrei, O. H. Aina, E. Y. Lau, F. C. Lightstone, R. Liu, K. S. Lam, M. J. Kurth, *J. Med. Chem.* **2009**, *52*, 14–19; c) M. Rusckowski, B. Fritz, D. J. Hnatowich, *J. Nucl. Med.* **1992**, *33*, 1810–1815.
[13] L. Ding, J. Stilwell, T. Zhang, O. Elboudwarej, H. Jiang, J. P. Selegue, P. A. Cooke, J. W. Gray, F. F. Chen, *Nano Lett.* **2005**, *5*, 2448–2464.
[14] J. A. Barltrop, T. C. Owen, A. H. Cory, J. G. Cory, *Bioorg. Med. Chem. Lett.* **1991**, *1*, 611–614.
[15] a) M. V. Berridge, A. S. Tan, *Arch. Biochem. Biophys.* **1993**, *303*, 474–482; b) A. H. Cory, T. C. Owen, J. A. Barltrop, J. G. Cory, *Cancer Commun.* **1991**, *3*, 207–212.
[16] T. L. Riss, R. A. Moravec, *Mol. Biol. Cell* **1992**, *3*, 184a.
[17] a) M. K. French, S. E. Creager, *Langmuir* **1998**, *14*, 2129–2133; b) C. D. Bain, E. B. Troughton, Y. T. Tao, J. Evall, G. M. Whitside, R. G. Nuzzo, *J. Am. Chem. Soc.* **1989**, *111*, 321.
[18] a) F. A. Arosa, O. de Jesus, G. Porto, A. M. Carmo, M. de Sousa, *J. Biol. Chem.* **1999**, *274*, 16917–16922; b) S. M. Claypool, B. M. Dickinson, M. Yoshida, W. I. Lencer, R. S. Blumberg, *J. Biol. Chem.* **2002**, *277*, 28038–28050; c) N. S. DeSilva, *Am. J. Respir. Cell Mol. Biol.* **2003**, *29*, 757–770; d) Z. Grabarek, J. Gergely, *Anal. Biochem.* **1990**, *185*, 131–135.
[19] J. Zhang, H. Zou, Q. Qing, Y. Yang, Q. Li, Z. Liu, X. Gou, Z. Du, *J. Phys. Chem. B* **2003**, *107*, 3712–3718.
[20] M. X. Pulikkathara, O. V. Kuznetsov, V. N. Khabashesku, *Chem. Mater.* **2008**, *20*, 2685–2695.
[21] A. Graja, I. Olejniczak, A. Bogucki, *J. Mol. Struct.* **2002**, *614*, 59–68.
[22] B. Laskowska, A. Łapiński, A. Graja, P. Hudhomme, *Chem. Phys.* **2007**, *332*, 289–297.
[23] E. V. Basiuk, V. A. Basiuk, J. G. Bañuelos, J. M. Saniger-Blesa, V. A. Pokrovskiy, T. Y. Gromovoy, A. V. Mischanchuk, B. G. Mischanchuk, *J. Phys. Chem. B* **2002**, *106*, 1588–1597.
[24] A. Palkar, A. Kumbhar, A. J. Athans, L. Echegoyen, *Chem. Mater.* **2008**, *20*, 1685–1687.
[25] A. S. Rettenbacher, B. Elliott, J. S. Hudson, A. Amirkhanian, L. Echegoyen, *Chem. Eur. J.* **2006**, *12*, 376–387.
[26] A. Kudelski, *Vib. Spectrosc.* **2005**, *39*, 200–213.
[27] *Infrared Spectroscopy: Fundamentals and Applications* (Ed.: B. Stuart), Wiley, New York, **2004**.
[28] M. Alvaro, P. Altienzar, P. De La Cruz, J. L. Delgado, V. Troiani, H. Garcia, F. Langa, A. Palkar, L. Echegoyen, *J. Am. Chem. Soc.* **2006**, *128*, 6626–6635.
[29] M. Furuki, J. Kameoka, H. G. Craighead, M. S. Isaacson, *Sens. Actuators B* **2001**, *79*, 63–69.
[30] D. P. Allison, P. Hinterdorfer, W. Han, *Curr. Opin. Biotechnol.* **2002**, *13*, 47–51.
[31] a) J. Zhang, A. Bilic, J. R. Reimera, N. S. Hush, J. Ulstrup, *J. Phys. Chem. B* **2005**, *109*, 15355–15367; b) M. Kawasaki, T. Sato, T. Yoshimoto, *Langmuir* **2000**, *16*, 5409–5417.
[32] I. Horcas, R. Fernandez, J. M. Gomez-Rodriquez, J. Colchero, J. M. Gomez-Herrero, A. M. Baro, *Rev. Sci. Instruments* **2007**, *78*, 013705.
[33] a) J. J. Gooding, R. Wibowo, J. Liu, W. Yang, D. Losic, S. Orbons, F. J. Meams, J. G. Shapter, D. B. Hibbert, *J. Am. Chem. Soc.* **2003**, *125*, 9006–9007; b) P. Kumar, S. Karmakar, H. B. Bohidar, *J. Phys. Chem. A* **2008**, *112*, 15113–15121.
[34] a) Y.-S. Chen, J.-H. Huang, *Diamond Relat. Mater.* **2009**, *18*, 516–519; b) B. S. Flavel, J. Yu, A. V. Ellis, J. G. Shapter, *Electrochim. Acta* **2009**, *54*, 3191–3198.
[35] K. Nozawa, C. Osono, M. Sugawara, *Sens. Actuators B* **2007**, *126*, 632–640.
[36] G. Reiss, F. Schneider, J. Vancea, H. Hoffman, *Appl. Phys. Lett.* **1990**, *57*, 867–869.
[37] X. Cui, R. Pei, Z. Wang, F. Yang, Y. Ma, S. Dong, X. Yang, *Biosens. Bioelectron.* **2003**, *18*, 59–67.
[38] K. A. Peterlinz, R. Georgiadis, T. M. Herne, M. J. Tarlov, *J. Am. Chem. Soc.* **1997**, *119*, 3401–3402.
[39] *Surface Plasmon Resonance Measurements of ultrathin organic films at electrode surfaces: From Electroanalytical Chemistry: A series of Advances, Vol. 20* (Eds.: A. J. Bard, I. Rubinstein), Marcel Dekker, New York, **1996**.
[40] a) I.-K. Park, H. A. von Recum, S. Jiang, S. H. Pun, *Langmuir* **2006**, *22(20)*, 8478–8484; b) J. Liu, R. Lauterbauch, H. Paulsen, W. Knoll, *Langmuir* **2008**, *24*, 9661–9667; c) O. Crespo-Biel, C. W. Liu, B. J. Ravoo, D. N. Reinhandt, J. Huskens, *J. Am. Chem. Soc.* **2006**, *128*, 17024–17032.
[41] a) E. Hutter, J. H. Fendler, D. Roy, *J. Phys. Chem. A* **2001**, *105*, 11159–11168; b) F. Wang, J. Wang, X. Liu, S. Dong, *Talanta* **2008**, *77*, 628–634; c) Y. Teramura, Y. Arima, H. Iwata, *Anal. Biochem.* **2006**, *357*, 208–215; d) C. Noguez, *J. Phys. Chem. C* **2007**, *111*, 3806–3819; e) A. J. Haes, S. Zou, G. C. Schatz, R. P. Van Duyne, *J. Phys. Chem. A* **2004**, *108*, 6961–6968.
[42] a) C. Zhao, Y. Song, J. Ren, X. Qu, *Biomaterials* **2009**, *30*, 1739–1745; b) I. V. Bondarev, K. Tatur, L. M. Woods, *Opt. Commun.* **2009**, *282*, 661–665.
[43] C. R. Evans, T. A. Spurlin, B. L. Frey, *Anal. Chem.* **2002**, *74*, 1157–1164.
[44] A. N. Kirschner, B. F. Erlanger, S. R. Wilson, Eight Foresight Conference on Molecular Nanotechnology conference, Bethesda, **2000**.
[45] I. Cheiken, S. Rose, R. Karlsson, *Anal. Biochem.* **1991**, *192–199*, 197–210.
[46] L. Fägerstam, A. Karlsson, R. Karlsson, B. Persson, I. Ronneberg, *J. Chromatogr.* **1992**, *597*, 397–410.
[47] E. Stenberg, B. Persson, H. Roos, C. Urbaniczky, *J. Colloid Interface Sci.* **1991**, *143*, 513–526.
[48] a) B. L. Frey, C. E. Jordan, S. Kornguth, R. M. Corn, *Anal. Chem.* **1995**, *67*, 4452–4457; b) R. C. Ebersole, J. A. Miller, J. R. Moran, M. D. Ward, *J. Am. Chem. Soc.* **1990**, *112*, 3239–3241.
[49] A. Schmidt, J. Spinke, T. Bayerl, E. Sackmann, W. Knoll, *Biophys. J.* **1992**, *63(5)*, 1385–1392.
[50] a) V. L. Kuznetsov, M. N. Aleksandrov, I. V. Zagoruiko, A. L. Chuvilin, E. M. Moroz, V. N. Kolomiichuk, *Carbon* **1991**, *29*, 665–668; b) V. L. Kuznetsov, A. L. Chuvilin, Y. V. Butenko, I. Y. Malkov, V. M. Titov, *Chem. Phys. Lett.* **1994**, *222*, 343–348.

Received: November 30, 2009
Published online: March 25, 2010

